RSC Advances

ROYAL SOCIETY OF CHEMISTRY

www.rsc.org/advances

Defect driven ferromagnetism in SnO_2: A combined study using Density functional theory and positron annihilation spectroscopy

A. Sarkar[1], D. Sanyal[2,*], Palash Nath[3], Mahuya Chakrabarti[3], S Pal[3], S. Chattopadhyay[4], D. Jana[3] and K. Asokan[5]

[1]*Department of Physics, Bangabasi Morning College, 19 Rajkumar Chakraborty Sarani, Kolkata 700009, India*

[2]*Variable Energy Cyclotron Centre, 1/AF, Bidhannagar, Kolkata 700064, India*

[3]*Department of Physics, University of Calcutta, 92 Acharyya Prafulla Chandra Road, Kolkata 700009, India*

[4]*Department of Physics, Maulana Azad College, 8 Rafi Ahmed Kidwai Road, Kolkata 700013, India*

[5]*Inter University Accelerator Centre, Post Box 10502, Aruna Asaf Ali Marg, New Delhi 110067, India*

[*]dirtha@vecc.gov.in Tel: 0091-33-23184462; FAX: 0091-33-23346871

Abstract

Room temperature ferromagnetic ordering has been observed in high purity polycrystalline SnO_2 sample due to irradiation of 96 MeV oxygen ions. *Ab initio* calculation in the density functional theory indicates that tin vacancies are mainly responsible for inducing magnetic moment in SnO_2 whereas oxygen vacancies in SnO_2 do not contribute any magnetic moment. Positron annihilation spectroscopy has been employed to characterize the chemical identity of irradiation generated defects in SnO_2. Results indicate the dominant presence of Sn vacancies in O ion irradiated SnO_2. The irradiated sample turns out to be ferromagnetic at room temperature.

PACS: 75.50.Pp; 71.15.Mb; 78.70.Bj

Keywords: Magnetic semiconductor; Density-functional theory, Positron annihilation spectroscopy

1. Introduction

Defects are ubiquitous in solids. An insignificant amount of defects in a solid can significantly alter its electrical, optical and magnetic properties. In fact, defect induced ferromagnetism in a wide range of materials has become one of the most discussed issues in recent past[1-4]. In oxide semiconductors like ZnO and other related compounds, several defect configurations offer enormous possibilities to study defect induced phenomenon theoretically and experimentally[5,6]. Majority of the scientific efforts have been directed to find ferromagnetism in doped and undoped ZnO[7-9] whereas, relatively fewer investigations exist on similar other materials like TiO_2[10,11] and SnO_2. [12,13] The present theoretical and experimental work has been focused to investigate the role of defects in generating ferromagnetism in SnO_2. SnO_2 is a wide band gap (~ 3.6 eV at room temperature) n-type semiconductor. In recent times, the occurrence of room temperature ferromagnetic ordering in undoped SnO_2 has been reported[14-17]. Espinosa et al. have indicated[15] that Sn vacancy (V_{Sn}) is responsible for inducing ferromagnetism in SnO_2 while Chang et al. favored[16] the key role of oxygen vacancies (V_O) for the same. Yuan et al. have found[17] that vacancy defects at grain surfaces in nanocrystalline SnO_2 control saturation magnetization (M_s). In SnO_2 nanowires, strong and tunable ferromagnetic response by ultraviolet light irradiation has been observed.[18] In the present effort, first principles DFT calculation has been adopted to observe the effect of V_{Sn} and V_O on the electronic structure of SnO_2. DFT results predict that V_{Sn}s are responsible for inducing ferromagnetism in SnO_2. On the experimental side, defects in SnO_2 have been created by 96 MeV oxygen beam irradiation. Positron annihilation spectroscopic (PAS) investigation reveals the abundance of Sn vacancies in the irradiated (ferromagnetic)

material. It is worth mentioning that PAS spectroscopy is very much sensitive to vacancy type open volume defects in solid materials.[2,6,19]. Particularly, in oxide semiconductors like ZnO and related materials, it efficiently probes cation vacancies with sub ppm accuracy[20].

Doppler broadening of the electron-positron annihilation radiation line shape (DBEPARL) measurement technique is useful to study the momentum distribution of electrons in a material. Depending on the electron momentum (p), the 511 keV γ-rays (electron–positron annihilated) are Doppler shifted by an amount $\pm\Delta E = p_L c/2$ in the laboratory frame, where p_L is the component of the electron momentum (p) along the direction of measurement[19]. Using high energy resolution HPGe (high purity germanium) detectors, one can measure the Doppler shift of the 511 keV γ-ray spectrum. In this spectrum, the region away from 511 keV photo peak is formed due to annihilation of positrons with higher momentum core electrons of the constituent atoms of the sample. Energy (or momentum) of such core electrons are element specific. So by analyzing the DBEPARL spectrum, identification of the vacant atomic sites can be done. But due to large background in the γ-ray spectrum the analysis of high p_L region becomes cumbersome and unambiguous. Use of the two detectors in coincidence (henceforth will be called CDBEPARL technique) is necessary to suppress the background in measured Doppler broadened spectrum and the contributions of higher momentum core electrons in the spectrum can be estimated[2,19,20].

2. Experimental outline

As received 99.996 % pure (Alfa Aesar, Johnson Mathey, Germany) SnO_2 powder has been used in this work. The powder has been pelletized and annealed at 700^o C before irradiation.

The magnetization measurements were done in a MPMS-XL SQUID (superconducting quantum interference device; Quantum Design) magnetometer.

For CDBEPARL measurement, 10 μCi ^{22}Na source of positrons (enclosed between ~ 1.5 μm thin nickel foils) has been sandwiched between two identical pellets. Electron-positron annihilated 511 keV gamma ray lineshape measurements have been carried out using two identical HPGe detectors (Efficiency: 12 % ; Type : PGC 1216sp of DSG, Germany) having energy resolution of 1.1 keV at 514 keV of ^{85}Sr. CDBEPARL spectra have been recorded in a dual ADC based - multiparameter data acquisition system (MPA-3 of FAST ComTec., Germany) having energy per channel – 146 eV. The peak to background ratio of this measurement system with ± ΔE selection is ~ 10^5:1. The CDBEPARL spectrum has been analyzed by evaluating the ratio curve analysis[19,20]. In each CDBEPARL spectrum the *S*-parameter[19] is calculated as the ratio of the counts in the central area of the 511 keV photo peak (| 511 keV - E_γ | ≤ 0.85 keV) and the total area of the photo peak (| 511 keV - E_γ | ≤ 4.25 keV). Defects in SnO_2 were created by using 96 MeV $^{16}O^{8+}$ ions from 15 UD pelletron at IUAC, New-Delhi. The irradiation fluence is 3.3 × 10^{13} ions/cm^2. The beam is uniformly scanned on the sample area of 1 cm × 1 cm.

3. Theoretical methodology

Defect induced modification of magnetic property of the SnO_2 have been investigated theoretically by studying the spin polarized density of states as calculated by the *ab-initio* density functional theoretical approach[21-23].

The theoretical calculations have been carried out in the frame work of the *ab-initio* density functional theory using the code MedeA VASP[24-27] based on linear basis set expansion. Super cell size is 2×3×3 *i.e.,* 108 atoms are taken for simulation with periodic boundary condition along the lattice vectors. All the structures are geometrically relaxed through the conjugate-gradient algorithm until all the unbalanced inter atomic forces are converged below 0.02 eV/Å. The unit cell size is obtained by geometrical optimization, which yields the lattice constant as, a = 4.7367 Å, b = 4.7367 Å and c = 3.1855 Å. All the simulations have been performed in the framework of generalized gradient approximation (GGA) with Perdew-Burke-Ernzerhof (PBE) exchange[28] correlation. The energy convergence criteria have been set to the value 10^{-4} eV and with the energy cut-off value of 400 eV. For Brillouin zone (BZ) sampling the Monkhorst-Pack parameter[29] are set by 3×2×3 *k*-points. The magnetic property of defect induced SnO_2 has been carried out by considering the spin polarized DFT calculation. The spin degrees of freedom fully relaxed during the simulation until the system converge to the spin polarized ground state. No initialization has been taken into account for the spin magnetic moment of the atoms or defects of the considered system. To create the defective system, a single Sn atom is removed from the system of 108 atoms yielding a Sn vacancy (V_{Sn}) concentration ~ 1.0% (Fig. 1) and similarly O atom also removed from the system to produce the O vacancy (V_O). For further calculation regarding the magnetic coupling (ferromagnetic or

antiferromagnetic) between the defects, two V_{Sn} are considered in the SnO_2 system at a distance 4.74 Å apart from each other and then ferromagnetic and antiferromagnetic ground state have been predicted through spin polarized DFT.

4. Results and discussion

The pristine and irradiated samples show standard x-ray diffractogram patterns of SnO_2 only (not shown). Little broadening of the diffraction lines due to irradiation has only been observed. The maximum penetration depth of 96 MeV O ions in SnO_2 is 54.6 μm (estimated using SRIM[30]). The maximum electronic energy loss by 96 MeV O ion is in the hundreds of eV/Å range (Fig. 2). Such values are much lower than the typical columnar defect generation threshold in insulators[31,32]. Thus mostly the point defects are generated in SnO_2 by the 96 MeV O ions. In order to obtain the vacancy concentration, one has to specify displacement threshold energy in SRIM. To the best of our knowledge, there is no theoretical or experimental data for the displacement threshold energy (E_d) of Sn or O in SnO_2. So in accordance with E_d values for Zn and O atoms in ZnO, these values have been taken as 57 eV (Ref. 33). SRIM predicts 3 V_{Sn} and 4 V_O in 2×10^4 atoms for a fluence of 10^{14} ions/cm^2. Due to such high concentration of defects, a significant modification of electronic properties is expected. However, it is to be noted that SRIM only predicts instantaneously generated defect concentration, no aftereffect such as dynamic recovery or defect complex formation is beyond the scope of such calculation.

Fig. 3 show the M vs. H curve, measured at room temperature for the oxygen irradiated SnO_2. The hysteresis loop (ferromagenic ordering) at room temperature for the the ion irradiated sample is relatively small (inset of Fig. 3) compared to the earlier

experimental results on Ar irradiated TiO_2[10] or mechanically milled SnO_2.[34] The coercieve field is only 75 Oe as is seen from the inset of Fig. 3.

The spin polarized density of states, as calculated by the *ab-initio* density functional theory, for the pristine SnO_2, V_O in SnO_2 and V_{Sn} in SnO_2 have been plotted in Figs. 4, 5 & 6 respectively. The symmetric spin polarized (for the up-spin and down-spin) density of states as depicted in Fig. 4 clearly indicates that the pristine SnO_2 yields zero magnetic moment. Due to the introduction of V_O in SnO_2 (Fig. 5) no magnetic moment have been emerged in SnO_2, while the present calculation shows an asymmetric spin polarized density of states (DOS) for V_{Sn}, which results a non-zero magnetic moment of 3.63 μ_B (Fig. 6). It is quite interesting to note that this value is in close agreement as predicted by Rahman, et al [Ref. 12]. In particular, the strong asymmetry between spin up and down state in SnO_2 with V_{Sn} exists very close to the Fermi energy (-2.5 eV to 0 eV). The defect formation energy of V_{Sn} and V_O has also been evaluated from the MedeA VASP software using the following definition;

$$E_f = E_d + E_a - E_p$$

where, E_f is the defect formation energy while E_d and E_p denote the total energy of the defective and pristine SnO_2 structures respectively. E_a is the energy of isolated Sn or O atom for V_{Sn} and V_O respectively. From the defect formation energy as shown in the Table 1, it can be concluded that the formation of V_O is energetically favorable than the V_{Sn}. However, non-equilibrium processes like ion irradiation as done here, abundant V_{Sn} can also appear in the system.

To investigate the interaction between the magnetic moments for a fixed defect-defect distance, we have further carried out the calculations with the two magnetization configurations, e.g., ferromagnetic (FM) and antiferromagnetic (AFM) states, respectively. The distance between the two defect sites in the supercell is taken to be 4.74 Å. The atomic positions in both FM and AFM cases have been fully optimized and the total energy has been computed. It has been found that the FM state is the ground state and its energy is roughly ~ 96 meV lower than that of the AFM state.

The implantation depth for the positrons from radioactive ^{22}Na is given by $P(x) = \eta \exp(-\eta x)$, where x is the distance measured from the surface of the sample from where the positrons penetrate inside the sample. $1/\eta$ is the characteristic penetration depth of a positron with specific energy (E). One can calculate $1/\eta$ which is approximately $(E_{max})^{1.4}/16\rho$ in cm, if E is expressed in MeV and ρ is the density of the material in gm/cm^3 (Ref. 35). E_{max} is the maximum energy of the emitted positrons, e.g., for ^{22}Na, E_{max} is ~ 0.54 MeV. In SnO_2 with density 5.56 gm/cm^3 (taking 80 % of the ideal density 6.95 gm/cm^3 for porous sample), $1/\eta$ comes out to be ~ 47 μm. It has been earlier mentioned that the depth of the irradiated region, as estimated by SRIM, is ~ 54.6 μm. So majority of the positrons will annihilate in damaged region of the irradiated sample. It is well known that the so called *S*-parameter represents the annihilation fraction of positrons with low energy electrons[19,35]. Increase of *S*-parameter represents enhanced positron annihilation at open volume defects. The *S*-parameter values of the pristine and irradiated materials are 0.5440 and 0.5457 respectively. Ratio curve analysis reveals that such open volumes in the irradiated sample are predominantly V_{Sn} type. Fig. 7 shows the area normalized ratio curve of the CDBEPARL spectrum of oxygen ion irradiated SnO_2 with

the same of pristine SnO_2. The dip in the ratio curve at momentum (p_L) value of 18×10^{-3} $m_o c$ indicates less annihilation of positrons with the higher momentum core electrons of Sn. Assuming positrons are thermalized before annihilation and using Virial theorem approximation (in the atom the expectation value of the kinetic energy of an electron, E_{kin}, is equal to the binding energy of the electron), one can calculate the E_{kin} using $p_L = (2\ m_0\ E_{kin})^{1/2}$ (Ref. 36). Here m_0 is the rest mass of an electron. The dip position in the ratio curves correspond to E_{kin} = 82.8 eV. This value of E_{kin} nicely agrees with the binding energy of Sn 4p core electrons (~ 83.6 eV).[37] As a consequence, presence of stable Sn vacancies in the 96 MeV O irradiated SnO_2 can now be concluded.

In the light of our results, decreasing trend of ferromagnetic moment with high temperature annealing[14,17] of SnO_2 nanoparticles can now be understood in the following way. Above 400 ^oC annealing grain boundary defects starts to recover and average grain size is increased[17,38]. The situation of nano-SnO_2[38] is very similar to that of nano-ZnO.[9,39] In both cases, cation vacancies at the grain surfaces start recovering above certain annealing temperature (300-400 ^oC). Of course, the concentration of singly ionized oxygen vacancies may also decrease[14] due to high temperature annealing, however, our DFT calculations indicate that the primary reason for the decay of ferromagnetic moment is the decrease of V_{Sn}. In fact, as is seen in ZnO, any extended disorder with several vacancy agglomerates either at grain boundaries[40] or at irradiated regions[7] can act as background defect network necessary for ferromagnetic interaction. Already it has been found that formation of V_{Sn} is more probable compared to V_O in truncated SnO_2 surfaces (as in nanosheets[41]). Similar phenomenon is very much likely in the vicinity of extended disorders in bulk SnO_2. This contention fits well with the experimental report of

increasing ferromagnetic moment of SnO_2 powder[34] with increasing hours of mechanical milling (which add net disorder in the system[39]). PAS results confirm the presence of cation vacancies in the core of such disorder, generated either by ion irradiation (as is here in O irradiated SnO_2) or in mechanically milled ZnO.[39] More investigation on the formation, chemical nature and role of vacancy clusters in SnO_2 would be encouraging.

Conclusion

Combining theoretical and experimental study, we have shown that occurrence of room temperature ferromagnetism in SnO_2 is due to Sn vacancies. The present methedology will serve for a conclusive identification of chemical nature of open volume defects in oxide and other compound semiconducting materials.

Acknowledgements

P. Nath acknowledges the financial assistance from Council of Scientific and Industrial Research (CSIR), Govt. of India. S. Pal acknowledges University Grants Commission (UGC), Govt. of India for providing his RFSMS fellowship.

References

1 A. Sundaresan, R. Bhargavi, N. Rangarajan, U. Siddesh and C. N. R. Rao, *Phys. Rev. B*, 2006, **74**, 161306(R).

2 D. Sanyal, M. Chakrabarti, T. K. Roy and A. Chakrabarti, *Phys. Lett. A*, 2007, **371**, 482.

3 M. Venkatesan, C. B. Fitzgerald, and J. M. D. Coey, *Nature*, 2004, **430**, 630.

4 A. Majumdar, S. Chowdhury, P. Nath and D. Jana, *RSC. Adv*., 2014, 4, 32221; P. Nath, A. Chakraborti and D. Sanyal, *RSC Adv.*, 2014, **4**, 45598.

5. J. Bang, Y. Kim, C.H. Park, F. Gao and S.B. Zhang, *Appl. Phys. Lett*., 2014, **104**, 252101.

6 S. Dutta, S. Chattopadhyay, A. Sarkar, M. Chakrabarti, D. Sanyal and D. Jana, *Prog. Mater. Sci.*, 2009, **54**, 89.

7 S. Mal, S. Nori, J. Narayan, J. T. Prater and D. K. Avasthi, *Acta Mater*., 2013, **61**, 2763.

8 B. Sieber, J. Salonen, E. Makila, M. Tenho, M. Heinonen, H. Huhtinen, P. Paturi, E. Kukk, G. Perry, A. Addad, M. Moreau, L. Boussekey and R. Boukherroub, *RSC Adv*. 2013, **3**, 12945.

9 S. Ghosh, A. Sarkar, S. Chattopadhyay, M. Chakrabarti, D. Das, T. Rakshit, S. K. Ray and D. Jana, *J. Appl. Phys.* 2013, **114**, 073516.

10 D. Sanyal, M. Chakrabarti, P. Nath, A. Sarkar, D. Bhowmick, A. Chakrabarti, *J. Phys. D: Appl. Phys.*, 2014, **47**, 025001.

11 M. Parras, Á. Varela, R. Cortés-Gil, K. Boulahya, A. Hernando and J. M. González-Calbet, *J. Phys. Chem. Lett*., 2013, **4**, 2171; S. Zhou, E. Čižmár, K. Potzger, M. Krause, G. Talut, M. Helm, J. Fassbender, S. A. Zvyagin, J. Wosnitza and H. Schmidt, *Phys. Rev. B*, 2009, **79**, 113201.

12. G. Rahman, *Phys. Rev. B, 2008, **78**,* 184404.

13 J. M. D. Coey, A. P. Douvalis, C. B. Fitzgerald and M. Venkatesan, *Appl. Phys. Lett*., 2004, **84**, 1332.

14 V. B. Kamble, S. V. Bhat and A. M. Umarji, *J. Appl. Phys*., 2013, **113**, 244307.

15 A. Espinosa, N. Sánchez , J. Sánchez-Marcos , A. de Andrés , and M. Carmen Muñoz, *J. Phys. Chem. C*, 2011, **115**, 24054.

16 G. S. Chang, J. Forrest, E. Z. Kurmaev, A. N. Morozovska, M. D. Glinchuk, J. A. McLeod, A. Moewes, T. P. Surkova, N. H. Hong, *Phys. Rev. B*, 2012, **85**, 165319.

17 C. Zhi-Yuan, C. Zhi-Quan, P Rui-Kun and W. Shao-Jie, *Chin. Phys. Lett*., 2013, **30**, 027804.

18 S. Bhaumik, A. K. Sinha, S. K. Ray A. K. Das, *IEEE Trans. Magnetics*, 2014, **50**, 1.

19 M. Chakrabarti, A. Sarkar, S. Chattopadhyay, D. Sanyal, A. K. Pradhan, R. Bhattacharya and D. Banerjee, *Solid State Commun*., 2003, **128**, 321; S. Dutta, M. Chakrabarti, S. Chattopadhyay, D. Jana, D. Sanyal, and A. Sarkar, *J. Appl. Phys*., 2005, **98**, 053513.

20 A. Sarkar, M. Chakraborti, D. Sanyal, D. Bhowmick, S. Dechoudhury, A. Chakrabarti, T. Rakshit and S.K. Ray, *J. Phys.: Condens. Matter*, 2012, **24**, 325503; D.J. Keeble, S. Wicklein, R. Dittmann, L. Ravelli, R. A. Mackie and W. Egger, *Phys. Rev. Lett*., 2010, **105,** 226102.

21 U. Bach, D. Lupo, P. Comte, J. E. Moser, F. Weissortel, J. Salbeck, H. Spreitzer and M. Gratzel, *Nature*, 1998, **395**, 583.

22 B Oregan and M. Gratzel, *Nature*, 1991, **353**, 737.

23 A. Hagfeldt, G. Boschloo, L. Sun, L. Kloo and H. Pettersson, *Chem. Rev.*, 2010, **110**, 6595.

24 G. Kresse and J. Hafner, *Phys. Rev. B*, 1993, **47**, 558.

25 G. Kresse and J. Hafner, *Phys. Rev. B*, 1994, **49**, 14251.

26 G. Kresse and J. Furthmüller, *Comput. Mater. Sci.*, 1996, **6**, 15.

27 G. Kresse and J. Furthmüller, *Phys. Rev. B*, 1996, **54**, 11169.

28 J. P. Perdew, K. Burke, and M. Ernzerhof, *Phys. Rev. Lett.*, 1996, **77**, 3865; J. P. Perdew, K. Burke, M. Ernzerhof, *Phys. Rev. Lett.*, 1997, **78,** 1396.

29 H. J. Monkhorst and J. D. Pack, *Phys. Rev. B*, 1976, **13**, 5188.

30 J. Ziegler, J. Biersack, and U. Littmark, *The Stopping and Range of Ions in Matter* (Pergamon, New York, 1985); SRIM 2000 code, www.srim.org

31 G. Szenes, *Phys. Rev. B*, 1995, **51**, 8026.

32 N. Ishikawa, S. Yamamoto and Y. Chimi, *Nucl. Instrum. Methods B*, 2006, **250**, 250.

33 D. R. Locker and J. M. Meese, *IEEE Trans. Nucl. Sci.*, 1972, **19**, 237.

34 S. Shi, D. Gao, Q. Xu, Z. Yang, D. Xue, *RSC Adv*., 2014, **4**, 45467.

35 R. Krause-Rehberg and H. S. Leipner, *Positron Annihilation in Semiconductors* (Springer, Verlag, Berlin, 1999).

36 U. Myler and P. J. Simpson, *Phys. Rev. B*, 1997, **56**, 14303.

37 www.webelements.com

38 C. H. Shek, J.K.L. Lai and G. M. Lin, *J. Phys. Chem. Solids*, 1999, **60**, 189.

39 S. Dutta, S. Chattopadhyay, D. Jana, A. Banerjee, S. Manik, S. K. Pradhan, M. Sutradhar, A. Sarkar, *J. Appl. Phys*., 2006, **100**, 114328; S. Dutta, S. Chattopadhyay, M. Sutradhar, A. Sarkar, M. Chakraborti, D. Sanyal, D. Jana, *J. Phys.: Condens. Matter*, 2007, **19**, 236218.

40 R. Podila, W. Queen, A. Nath, J. T. Arantes, A. L. Schoenhalz, A. Fazzio, G. M. Dalpian, J. He, S. J. Hwu, M. J. Skove and A. M. Rao, *Nano Lett*., 2010, **10**,1383.

41 G. Rahman, V. M. García-Suárez and J. M. Morbec, *J. Mag. Mag. Mater*., 2013, **328**, 104.

Figure and Table captions

Table 1 Theoretically calculated parameters (using DFT) for the non-defective SnO_2, oxygen vacancy (V_O) incorporated SnO_2, and tin vacancy (V_{Sn}) incorporated SnO_2.

Fig. 1 Magnetization density of different SnO_2 systems. (a) The pristine SnO_2 structure showing no magnetism. (b) Oxygen vacancy (V_O) in SnO_2 system; (c) SnO_2 system with single Sn vacancy (V_{Sn}); highly localized magnetization is noticed around Sn vacancy due to the nearest oxygen atoms. (d) Double Sn vacancy in SnO_2 system, the nearest oxygen atoms give rise to local magnetism. In the figures (b) – (d) the dotted circles represents the vacancy sites.

Fig. 2 Electronic and nuclear energy deposition of 96 MeV O^{8+} on SnO_2 as simulated by SRIM

Fig. 3 Room temperature magnetic hysteresis loop of 96 MeV O irradiated SnO_2. The inset shows the enlarged part near the zero field region.

Fig. 4 Spin polarized density of states for non-defective SnO_2 ($Sn_{16}O_{32}$)

Fig. 5 Spin polarized density of states for SnO_2 with oxygen vacancy ($Sn_{16}O_{31}$)

Fig. 6 Spin polarized density of states for SnO_2 with Sn vacancy ($Sn_{15}O_{32}$)

Fig. 7 Ratio curve constructed from the CDBEPARL spectrum for irradiated SnO_2 with respect to the same for pristine sample.

Table 1 Theoretically calculated parameters (using DFT) for the non-defective SnO_2, oxygen vacancy (V_O) incorporated SnO_2, and tin vacancy (V_{Sn}) incorporated SnO_2.

System	Defect formation energy (eV)	Bond length (Å)	Magnetic moment (μ_B)
Pristine	0.0	1.952	0.0
V_O	8.69	1.842	0.0
V_{Sn}	16.0	1.884	3.63

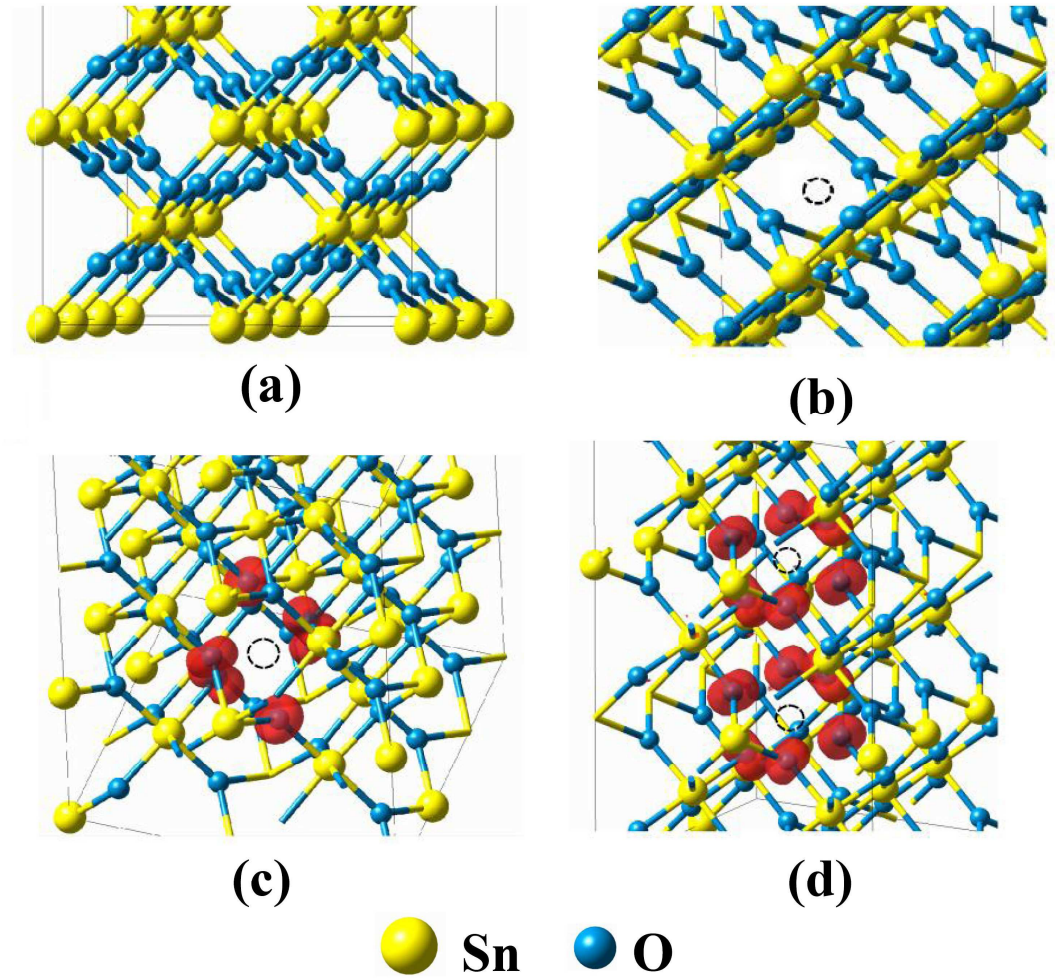

Fig. 1 Magnetization density of different SnO_2 systems. (a) The pristine SnO_2 structure showing no magnetism. (b) Oxygen vacancy (V_O) in SnO_2 system; (c) SnO_2 system with single Sn vacancy (V_{Sn}); highly localized magnetization is noticed around Sn vacancy due to the nearest oxygen atoms. (d) Double Sn vacancy in SnO_2 system, the nearest oxygen atoms give rise to local magnetism. In the figures (b) – (d) the dotted circles represents the vacancy sites.

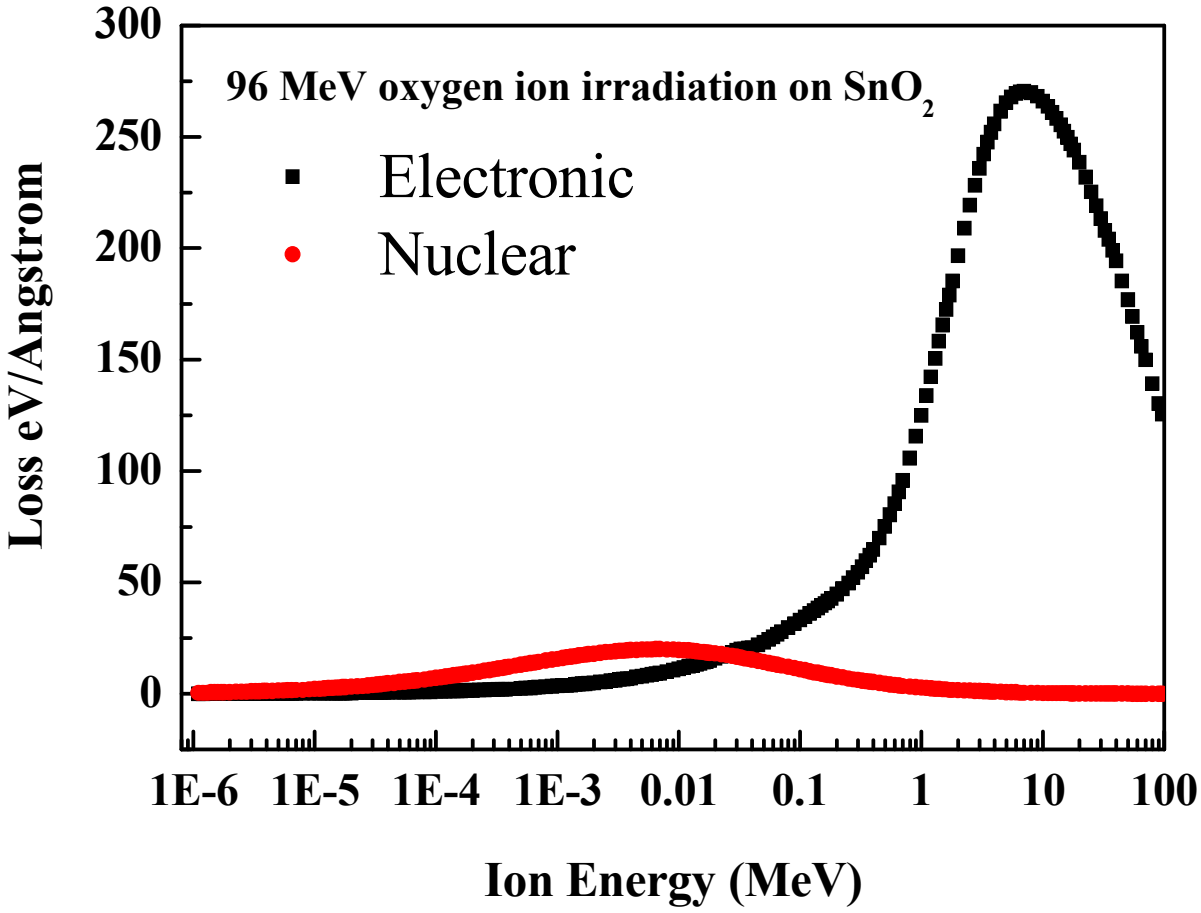

Fig. 2 Electronic and nuclear energy deposition of 96 MeV O^{8+} on SnO_2 as simulated by SRIM

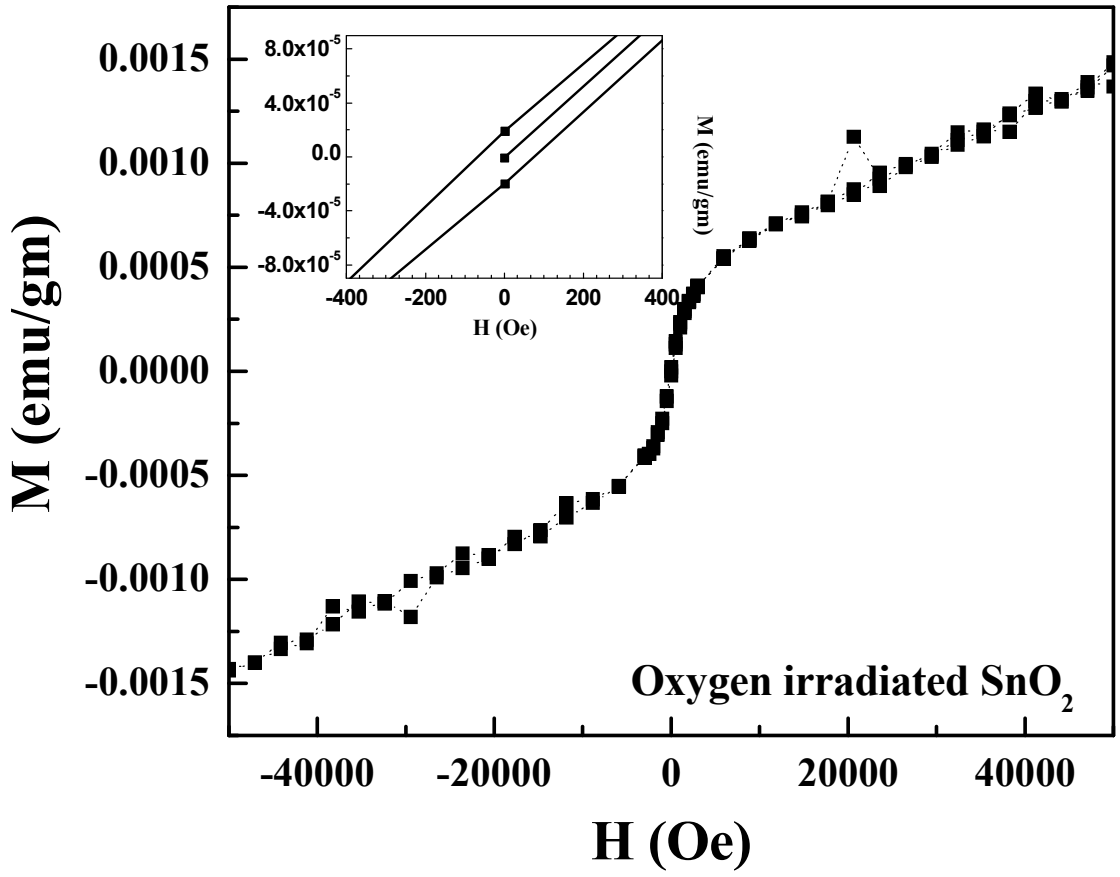

Fig. 3 Room temperature magnetic hysteresis loop of 96 MeV O irradiated SnO_2. The inset shows the enlarged part near the zero field region.

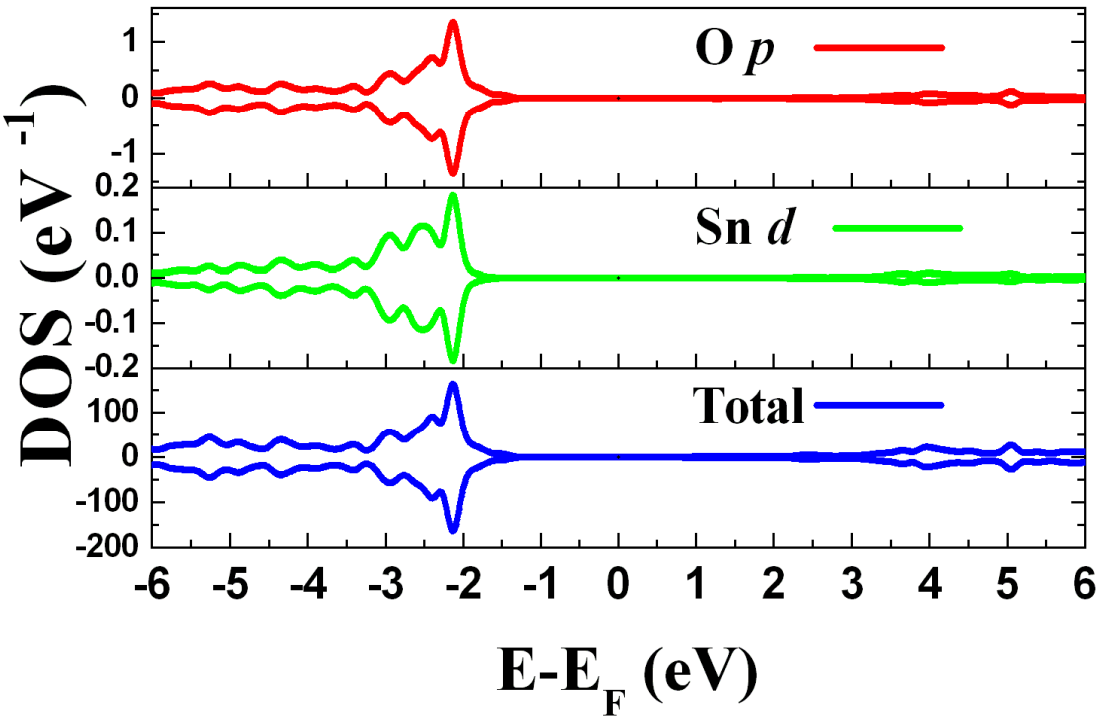

Fig. 4 Spin polarized density of states for non-defective SnO_2 ($Sn_{16}O_{32}$)

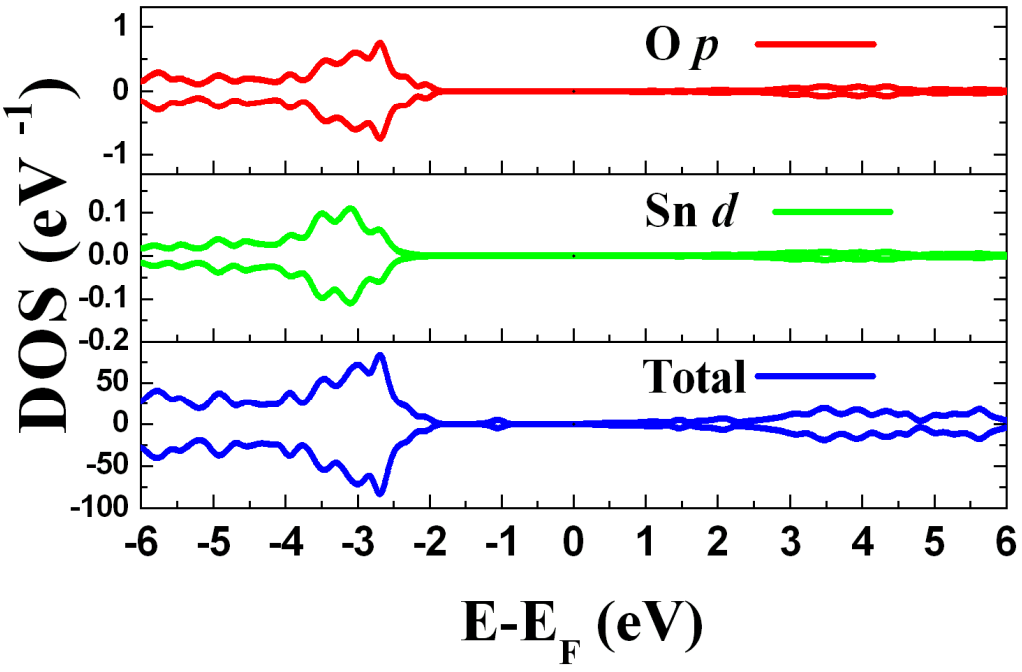

Fig. 5 Spin polarized density of states for SnO_2 with oxygen vacancy ($Sn_{16}O_{31}$)

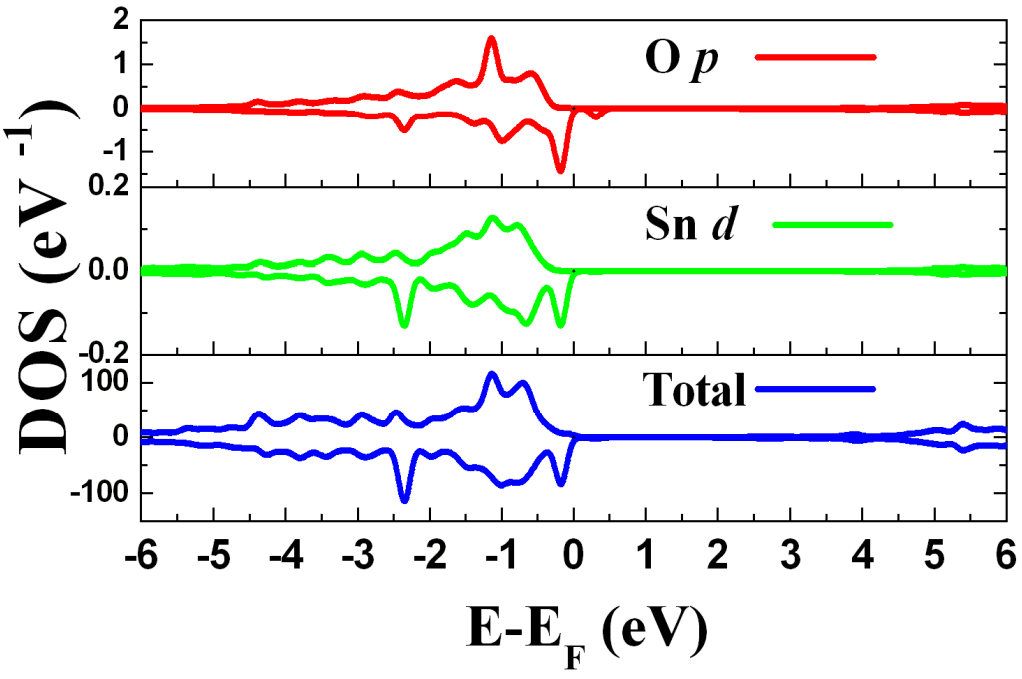

Fig. 6 Spin polarized density of states for SnO_2 with Sn vacancy ($Sn_{15}O_{32}$)

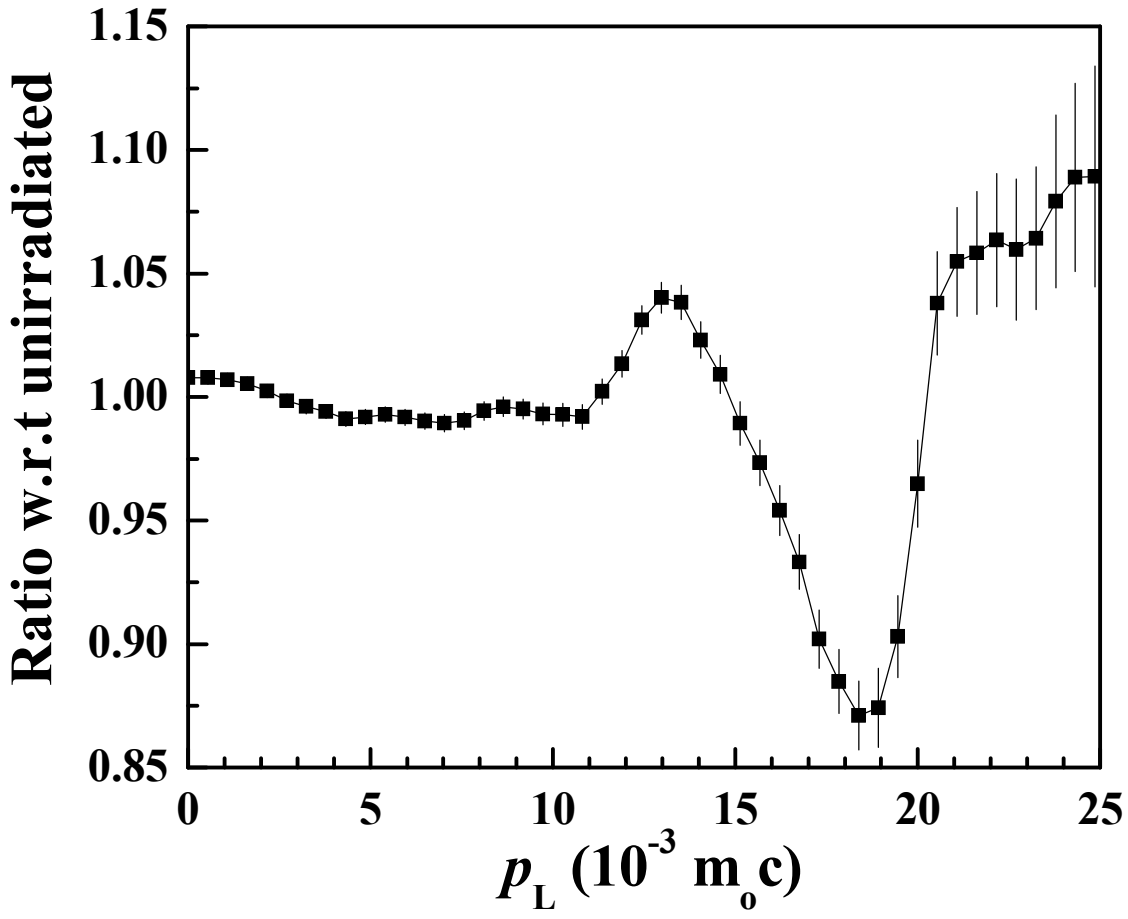

Fig. 7 Ratio curve constructed from the CDBEPARL spectrum for irradiated SnO_2 with respect to the same for pristine sample.

Room temperature ferromagnetic ordering has been observed in high purity polycrystalline SnO_2 sample due to irradiation of 96 MeV oxygen ions. *Ab initio* calculation in the density functional theory indicates that tin vacancies are mainly responsible for inducing magnetic moment in SnO_2 whereas oxygen vacancies in SnO_2 do not contribute any magnetic moment. Positron annihilation spectroscopy has been employed to characterize the chemical identity of irradiation generated defects in SnO_2. Results indicate the dominant presence of Sn vacancies in O ion irradiated SnO_2. The irradiated sample turns out to be ferromagnetic at room temperature.

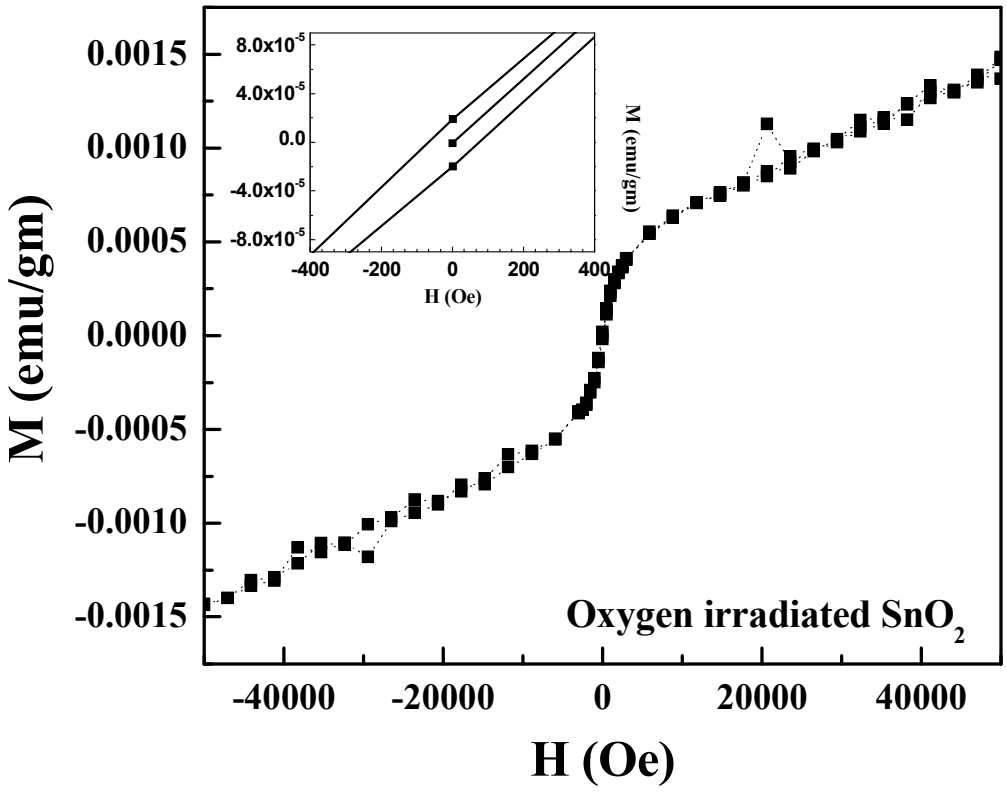

Room temperature magnetic hysteresis loop of 96 MeV O irradiated SnO_2. The inset shows the enlarged part near the zero field region.